ACS Catalysis

Research Article

pubs.acs.org/acscatalysis

# Modeling Catalyst Preparation: The Structure of Impregnated−Dried Copper Chloride on γ-Alumina at Low Loadings

Manuel J. Louwerse* and Gadi Rothenberg

Van't Hoff Institute for Molecular Sciences, University of Amsterdam, Postbus 94720, 1090 GS Amsterdam, The Netherlands

**ABSTRACT:** The structure of uncalcined atomically dispersed copper(II) chloride on γ-alumina is modeled with Density Functional Theory (DFT). Calculations are performed for the (110), (100), and (111) surfaces at several levels of hydration. The importance of the hydration and the uncertainties in the dehydration temperatures of the various γ-alumina surfaces are discussed. We find that both $Cu^{2+}$ and $Cl^-$ do not adsorb on the (111) surface of γ-alumina. Moreover, we show that additional water molecules are present on the copper ions, which are *not* part of the alumina hydration layer. A correct modeling of adsorbed metal ions should therefore include these additional water molecules. Regarding the chloride ions, we find that these prefer "sitting" on the copper ions, in contrast with reported results for uncalcined copper chloride. We explain this difference in terms of kinetic accessibility and predict the formation of $CuCl^+$ and $CuCl_2$ species during calcination. Validation laboratory experiments using temperature programmed desorption (TPD) and reduction (TPR) confirm the predicted repositioning of chloride ions upon moderate heating. Depending on the placement of the chlorides on the alumina surface or on the copper ions, the calculated structures compare well with experimental results before and after heating, respectively. The copper location and coordination in the former structure also applies to samples impregnated with copper(II) nitrate.

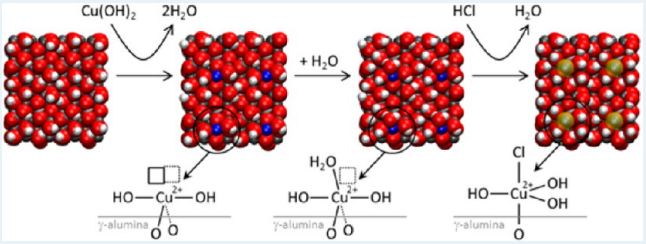


**KEYWORDS:** *hydration layer, gamma alumina, ion exchange, impregnation, oxychlorination, cupric ions, coordinated water, heterogeneous catalysis*

## INTRODUCTION

Many heterogeneous catalysts consist of nanoparticles of active material on a high surface area support. They are often prepared by impregnating the support with an aqueous solution of a catalyst precursor, followed by calcination and activation. However, obtaining a good and active catalyst in this way is far from trivial. Many small details in the preparation can strongly influence the results, and finding the right preparation procedure is often a matter of trial and error.[1−5]

Thus, connecting the preparation procedure to the final catalytic performance is a big challenge. To do so, we must understand the relations both between the preparation method and surface structure and between the surface structure and catalytic performance. Numerous studies in catalysis focus on the second part.[6−9] Here, we look at the first part, trying to understand the connection between the preparation process (the so-called "catalyst recipe") and structure by modeling the processes that occur during catalyst preparation.

In the case of impregnation, the catalyst preparation consists of the following steps: (i) impregnation, (ii) drying, (iii) calcination, and (iv) activation, followed by potential structural changes during the catalytic reaction itself (v). We will focus on the calcination step, during which the nanoparticles are formed. The key processes here are the diffusion of the metals and conversion of the precursors. To model these processes properly, one must have a good model of the structure *before* calcination. However, modeling the impregnation and drying steps themselves is difficult.[10,11] Here, we investigate whether the resulting structure can also be modeled directly by searching the thermodynamic optimum.

Note that our work concerns systems with a relatively low loading (ca. 1 atom/nm$^2$). Experimentally, provided that impregnation is performed carefully, the ions will spread over the surface as isolated monomeric species up to a certain loading.[12−21] Above this loading, precipitation of larger particles occurs. Because, also at high loadings, isolated species are always present on the surface, we choose to study those first.

Our model catalyst is copper(II) chloride on γ-alumina, an oxychlorination catalyst used in the production of vinyl chloride ($C_2H_3Cl$).[22,23] This process begins with chlorinating ethylene to 1,2-dichloroethane, followed by thermal cracking to the final product:

$$C_2H_4 + Cl_2 \rightarrow C_2H_4Cl_2 \quad (1)$$

$$C_2H_4Cl_2 \rightarrow C_2H_3Cl + HCl \quad (2)$$

To reduce the consumption of $Cl_2$ and the output of waste HCl, a third step was developed: the oxychlorination of ethylene to 1,2-dichloroethane, which is then fed back to step 2.

Received: October 1, 2012
Revised: May 15, 2013
Published: June 13, 2013

   dx.doi.org/10.1021/cs400253w | ACS Catal. 2013, 3, 1545−1554

Step 3 is where $CuCl_2$ on $\gamma$-alumina is used as a catalyst, often doped with KCl and $LaCl_3$ to improve activity and stability.[23−25]

$$C_2H_4 + 2HCl + \frac{1}{2}O_2 \rightarrow C_2H_4Cl_2 + H_2O \quad (3)$$

Despite the large volume of empirical data on this catalyst, we still do not know the precise structure of the copper species.[13,26−30] That said, the catalyst structure clearly differs for low and high loadings. Leofanti et al. performed a very thorough study of both structures for the case of pure $CuCl_2$, studying the changes that occur during drying, aging, and heating.[13,31] They found that for uncalcined samples up to a copper content of 0.95 wt % Cu/100 $m^2g^{-1}$ (0.90 Cu ions/$nm^2$), the copper and chloride ions sit isolated on the surface (the saturation point is roughly three times lower than for copper nitrate). The local surroundings of the ions were measured using EPR and EXAFS, showing that the copper ions had five oxygen neighbors at a distance of 1.94 ± 0.01 Å and zero chloride neighbors (see Figure 1).[13,32]

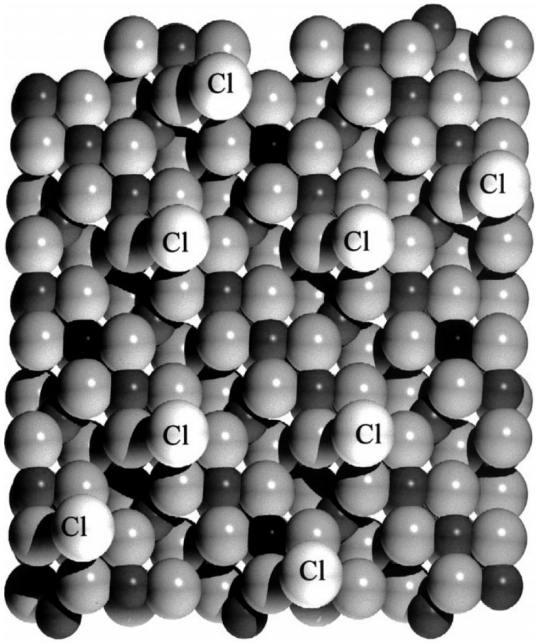


**Figure 1.** $CuCl_2$ on $Al_2O_3$ defective spinel (110) surface according to ref 13. Dark and light gray spheres are aluminum and oxygen atoms, black is copper, and white is chlorine. Reproduced with permission from ref 13. Copyright 2000 Elsevier.

However, as the precise structure of $\gamma$-alumina was unknown at the time, Leofanti et al. used a model of a spinel-type structure for summarizing their experimental results. Since then, the $\gamma$-alumina structure was modeled by several groups, concluding independently that it is not spinel-like.[33,34] Instead, the cations are highly disordered, with over 40% occupying nonspinel positions.[34] Digne et al. modeled the main surfaces for this structure, also taking into account different states of hydration at various temperatures.[35,36] As the $Al^{3+}$ cations are much more disordered than in Figure 1 and the alumina surfaces are hydrated at room temperature (and, as we will show, still partly hydrated even at calcination temperatures), the actual positions of $Cu^{2+}$ and $Cl^-$ ions on $\gamma$-alumina surfaces will differ from Figure 1.

Here, we started from Digne's $\gamma$-alumina surface model and modeled monomeric copper(II) chloride at various levels of hydration, comparing the results with Leofanti's experiments. We expect that the OH groups from the hydration layer will influence the bonding of the $Cu^{2+}$ and $Cl^-$ ions considerably.[37,38] Other examples of surface species influencing adsorption are Pt reconstruction and redispersion by hydrogen and chloride.[39,40] As (part of) the hydrating water leaves during calcination, the interactions of the copper and chloride ions with the surface will change. This will affect the further oxidation, diffusion, or desorption of these species. Establishing a good model of the uncalcined system at various hydration levels is thus essential for modeling the processes that occur during calcination. Our models can tell, in essence, where on the surface the different ions are situated, which can be compared with experimental results.

After describing the methods, we discuss first the prediction of dehydration temperatures and then the binding of copper and chloride ions on $\gamma$-alumina. For the copper ions, we find an interesting hydration effect. For the chloride ions, we find that the structure after drying with no copper−chloride contacts is a metastable structure, and upon heating the chlorides should move to the copper ions. Both the structures before and after heating are well described by our models. Lastly, we provide an experimental confirmation of this theoretical prediction.

## METHODS

**Computational.** All calculations were performed with the SIESTA code,[41,42] employing Density Functional Theory (DFT).[43,44] As we focus on surface adsorption, we used the revised Perdew−Burke−Ernzerhof (rPBE) functional.[45] Improved Troullier−Martins pseudopotentials[46] were used with input parameters taken from the Octopus project.[47] Relativistic corrections were applied for all atom types. For aluminum and copper, core corrections were applied with pseudocore radii of 0.92 bohr and 0.84 bohr, respectively. Numerical atomic orbital basis sets were optimized as described elsewhere.[48] The TZP (and TZ2P for aluminum) basis sets of ref 48 were used with Sankey-type cutoffs.[49] The density mesh cutoff was 100 Ry (plus 2-fold grid-cell sampling), unless otherwise stated. Optimizations were done with the conjugate gradient method, converged to 0.1 eV/Å. All calculations containing $Cu^{2+}$ were performed in the spin state $S = 1/2$.

The main crystal facets in $\gamma$-alumina are the (100), (110), and (111) surfaces, accounting for respectively 16%, 74%, and 10% of the surface area.[36] We used coordinates for these surfaces obtained from Digne et al.[33,35,36] This is a periodic slab model with 80−116 atoms (depending on the level of hydration) per unit cell. The slab thickness was 18.5 Å, 14.8 Å, and 10.8 Å for the fully hydrated (100), (110), and (111) surfaces, respectively. Perpendicular to the slab there is a layer of vacuum between the periodic repetitions of the structure. The total thickness of the unit cell was set to 29 Å, 25 Å, and 21 Å, respectively. An alternative "defect" structure with a more reactive aluminum site as proposed by Wischert et al.[50,51] was not explicitly included, as $Cu^{2+}$ does not bind to aluminum ions but to oxygen ions. For binding chloride, though, it was included implicitly, as it could form via our sampling procedure.

Because we used a different software package, a different DFT functional, and other different settings than Digne et al., we first reoptimized the alumina coordinates with our settings. The unit cell dimensions were optimized for the fully hydrated surfaces, using a density mesh cutoff of 200 Ry. Table 1 gives

**Table 1. Unit Cell Vectors after Reoptimization with the rPBE Functional, Compared to the Original PW91 Optimized Unit Cells**

| surface | unit cell vectors (in Å) | original unit cell vectors (in Å) |
|---|---|---|
| (100) | (5.91, −0.05, 0.00) | (5.57, 0.00, 0.00) |
| | (−0.07, 8.67, 0.00) | (0.00, 8.38, 0.00) |
| | (0.00, 0.00, 29.00) | (0.00, 0.00, 29.00) |
| (110) | (8.09, 0.00, 0.00) | (8.05, 0.00, 0.00) |
| | (0.00, 8.69, 0.00) | (0.00, 8.39, 0.00) |
| | (0.00, 0.00, 25.00) | (0.00, 0.00, 25.00) |
| (111) | (9.93, −0.03, 0.00) | (9.72, 0.01, 0.00) |
| | (−0.02, 8.62, 0.00) | (0.00, 8.38, 0.00) |
| | (0.00, 0.00, 21.00) | (0.00, 0.00, 21.00) |

the obtained unit cell vectors. For the partially hydrated and the unhydrated surfaces, the same cell parameters were used. Reoptimizing the alumina surface structures gave only minor changes in the hydrogen bond network.

To ensure identical density meshes as in the surface calculations, gas phase species (needed as zero for adsorption energies) were calculated three times, using all three sets of unit cell vectors given in Table 1. For the gas phase calculations with the (100) vectors, the *x* vector was doubled, avoiding spurious interactions with the periodic copies.

A good approach for finding the structure of adsorbed ions, without fully modeling the impregnation and drying processes, is ion exchange. Here, one begins with a hydrated support surface, exchanging protons with metal cations and hydroxyls with precursor anions.[52−54] In our case, this means that each $Cu^{2+}$ ion replaces two protons, and each $Cl^-$ replaces one $OH^-$. We defined the exchange energies according to the reactions in eqs 4 and 5:

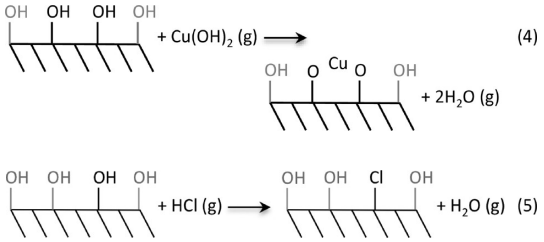


Note that these equations are not meant to describe the mechanism of ion exchange nor imply the involvement of gaseous $Cu(OH)_2$. This definition of the exchange energies is chosen because the energies of dissolved ions are not readily computationally accessible, and relative differences are not influenced by this definition. Here, we assume that the adsorption strength of the rest of the hydration layer is not influenced by the adsorption of copper or chloride. Our analysis cannot distinguish the actual interactions of these ions from potential indirect effects on the hydration layer.

We exchanged all eligible protons and hydroxyls one by one, optimized the structures, and selected the structure with the best energy as the likely structure of an ion on the hydrated support surface. Chloride ions were simply placed on the oxygen position of the exchanged $OH^-$. Following the results of Digne et al. for chloride on $\gamma$-alumina,[53] only primary hydroxyls were exchanged, plus any hydroxyl within 2.5 Å from the copper ion.

For the $Cu^{2+}$ cations, the situation is more complex: one cannot predict *a priori* which pairs of protons are likely to be replaced, nor where the metal ion will go (on the position of one of the exchanged protons, midway between the two, or elsewhere). Computing all the possible combinations of two hydrogen atoms and metal ion locations is impractical. Instead, we calculated all the combinations (using a 20-fold grid as possible Cu locations) only for one surface with a moderate number of hydrogen atoms (the (110) surface with three hydrating water molecules per unit cell) and then tested various schemes for decreasing the number of calculations needed. The best performing scheme was sampling only two possible (starting) positions for the copper, namely the position of either of the two replaced protons, while still sampling every pair of protons. This way, for the test surface, the largest deviation from the optimal structure was less than 0.15 eV.

Furthermore, we added additional water molecules on top of the $Cu^{2+}$ ion. If a water molecule binds stronger to the copper ion than to the alumina surface at a given level of hydration, this water molecule will be on the copper even on partially dehydrated surfaces at elevated temperatures or lowered pressures. As far as we know, for modeling metal ions on a support, we are the first to take into account the presence of water molecules that are coordinated to the adsorbed metal ion yet are not part of the hydration layer of the support. Note that such an additional water molecule can also be split into a $OH^-$ coordinated to the metal ion and a $H^+$ moving to one of the alumina oxygens, forming another hydration OH group.

Additional copper-coordinated water molecules were added by placing candidate O atoms on 56 positions around the copper ion and optimizing them with a simple Lennard-Jones force field (keeping all other atoms frozen). The resulting O positions were grouped, and only positions within 2.5 Å of the $Cu^{2+}$, with a negative binding energy, and more than 1.5 Å apart were selected. Hydrogen atoms were added opposite to the copper ion, either to form $H_2O$ or $OH^-$, in which case the other hydrogen was placed on any surface oxygen with no hydrogen, again giving several possibilities. All these structures were then optimized by DFT calculations. The result is a valid picture of the ions and atoms on the catalyst surface that can be correlated and compared with experimental studies.

Our overall method is depicted in Scheme 1: For each surface at each hydration level, all combinations of two hydrogen atoms were exchanged for one copper ion, placing the copper once on each H position. All the structures were then fully optimized. Then, the energetically best unique structures (copper locations more than 1.0 Å apart) were selected up to 1.0 eV above the best one. To these structures was added a water molecule (both unsplitted and splitted), and the structures were optimized again. To the best structures up to 0.5 eV was added another water molecule (again unsplitted and splitted), and then optimization took place. Then, for all unique structures with one copper and zero, one, or two additional water molecules, the best structures were selected again up to 0.7 eV, and each primary or metal-coordinated OH group was replaced with a chloride. Finally, to the best resulting optimized structures up to 0.5 eV, a second $Cl^-$ was added by replacing primary and metal-coordinated OH groups.

The thresholds of 1.0, 0.7, and 0.5 eV are needed because the best structures for a bare adsorbed ion are not necessarily the same as the best structure after adding water. The value of 0.7 eV is a rough estimate of the maximum relative energy change upon the addition of water. We have assumed that for second waters or chlorides there is more correlation with the best


dx.doi.org/10.1021/cs400253w | ACS Catal. 2013, 3, 1545−1554

**Scheme 1. Flowchart Showing the Step-by-Step Construction of the Models**[a]

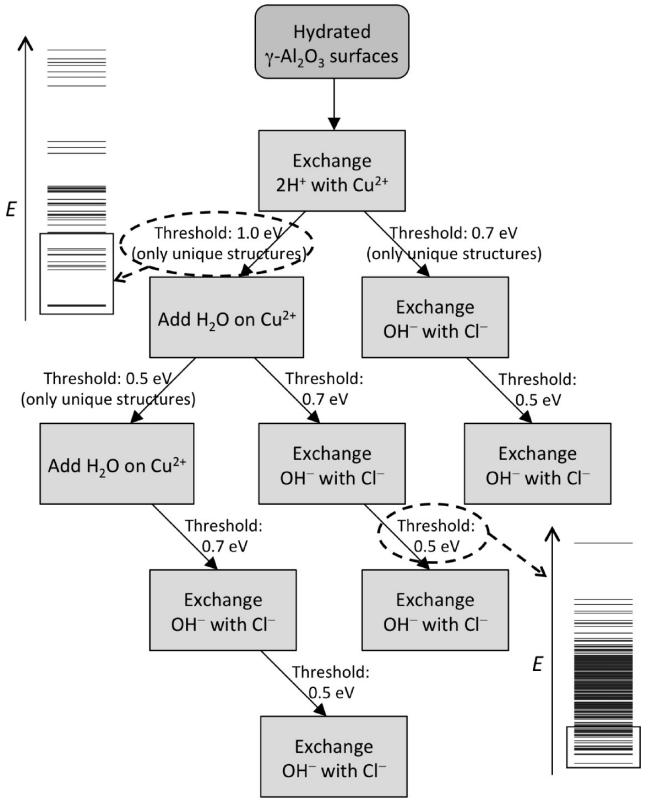


[a]To appreciate the lower threshold for second waters and chlorides, we show two examples of the energy levels of the constructed and the selected structures. These examples are given for the (110) surface with four water molecules per unit cell (5.7 $H_2O/nm^2$).

structures with only one water or chloride, hence the lower threshold of 0.5 eV.

**Experimental Section.** A copper chloride catalyst supported on $\gamma$-alumina with 1.5 wt % Cu (corresponding to 0.76 Cu ions/$nm^2$, ca. 15% below the saturation point of the surface) was prepared by wet impregnation. The support (1.02 g of $\gamma$-alumina; Ketjen CK300, 192 $m^2/g$) was mixed with 7 mL of aqueous solution of 40 mg of $CuCl_2 \cdot 2H_2O$ (Merck, 99%) and stirred for 24 h at room temperature. The solid catalyst was filtered and then dried in air at 105 °C for 48 h.

Temperature programmed desorption (TPD) and reduction (TPR) were run on a Thermo TPDRO 1100 instrument using a thermal conductivity detector (TCD). Before the detector, water is trapped and filtered out, so only compounds other than water were measured. Therefore, all measured desorbing compounds are interpreted as HCl. All measurements were done with samples of 60 mg, except for the TPR after TPD sample (24 mg). Before measuring the TPD or TPR, each sample was dried again for 1 h at 120 °C under a $N_2$ flow. TPD was measured under a 40 mL/min $N_2$ flow, heating with 10 K/min from 30 °C until 900 °C. TPR was measured under 5% $H_2$ in a $N_2$ flow (40 mL/min), heating at 10 K/min from 30 °C until 800 °C. All graphs were block-averaged over 50 points (50 s).

Pretreated samples were heated under a $N_2$ flow at 10 K/min to 400 °C, then kept at 400 °C for 1 h, and cooled back at −20 K/min before starting the TPD or TPR measurement.

## RESULTS AND DISCUSSION

**Dehydration Temperatures.** We modeled the copper and chloride binding on $\gamma$-alumina at several hydration levels, corresponding to different temperatures/pressures. When the temperature is raised, the hydration decreases. Therefore, it is important to know the actual hydration level under the process conditions. For this purpose, Digne et al. calculated surface free energy versus temperature plots.[36] Here, we reanalyze their (PW91) data taking into account the temperature dependence of the entropy and comparing with our data calculated with the rPBE functional. As the PW91 functional is known to overestimate adsorption,[45] the values from the PW91[36] and rPBE results may be considered as upper and lower bounds for the dehydration temperatures (rPBE may underestimate adsorption for weak adsorbates such as water).

We calculated dehydration temperatures using $\Delta H = T\Delta S$, comparing the water molecules adsorbed on the surface to gas phase water molecules at 1 atm of pressure. For gas phase molecules, the entropy is almost exclusively based on translational and rotational freedom. According to statistical mechanics, this leads to a temperature dependence (for nonlinear molecules) of $S = a + 4R \ln T$, where $R$ is the ideal gas constant and $a$ depends on the moments of inertia of the molecule. For water vapor, the entropy at 298 K and 1 atm is 188.7 J/mol K.[55] Finding the entropy of the adsorbed water molecules is more difficult. Recently, it was shown for smooth surfaces and inactivated desorption processes that adsorbed molecules at their desorption temperature behave like a 2D gas and have almost 2/3 of their gas phase entropy.[56] However, for our surfaces with many different binding sites, we expect the adsorbed molecules to be more restricted than that. In that case, the main entropy contribution is the librational (i.e., restricted rotational) freedom of the chemisorbed molecule. We have assumed that the librational freedom, and thus the entropy, of the water molecules at their desorption temperature equals that of ice at its melting temperature, i.e., 38.1 J/mol K.[55] The resulting dehydration temperatures in Figure 2 show a significant difference between the PW91 and rPBE results.

In the study of Leofanti et al., the samples were dried at room temperature and measured at $1.3 \times 10^{-6}$ bar.[13] This is

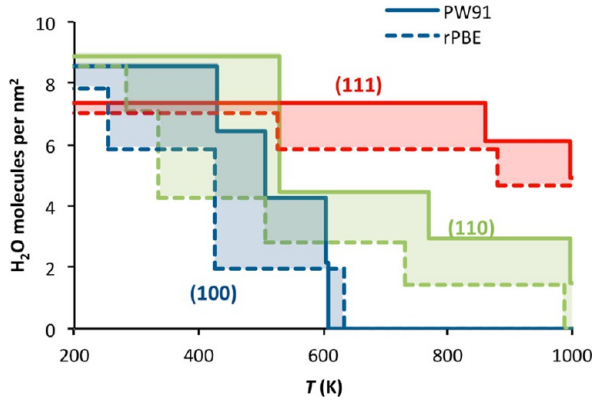


**Figure 2.** Hydration level of $\gamma$-alumina surfaces at increasing temperatures and 1 atm of pressure, calculated with the PW91 (solid lines, reanalyzed from the data of ref 36) and the rPBE functionals (dashed lines). Dehydration temperatures calculated using these two functionals may be considered as upper and lower bounds, respectively. The uncertainty on the $y$ axis reflects the differences in the unit cell sizes.


dx.doi.org/10.1021/cs400253w | ACS Catal. 2013, 3, 1545−1554

comparable to drying at 520 K at atmospheric pressure. Assuming that the correct dehydration temperatures are the means of the PW91 and the rPBE results, this suggests that these samples contained ca. four water molecules/nm$^2$ on the (100) and (110) surfaces and were still fully hydrated on the (111) surfaces.

We also considered the stability of the $\gamma$-alumina surface during impregnation, as the surface may partially be turned into Bayerite by the water. In practice, impregnation times range from a few hours up to 24 h, and $\gamma$-alumina is stable in water for such times.[57] Moreover, the presence of metal ions on the surface tends to increase the stability.[58]

**$Cu^{2+}$ on $\gamma$-Alumina.** We modeled $Cu^{2+}$ ions on the (100), (110), and (111) surfaces of $\gamma$-alumina at various levels of hydration. However, for none of the surfaces was the experimentally observed octahedral copper coordination (with five oxygen neighbors and one vacancy) obtained. In all cases, we found structures with three or four oxygen neighbors, either in a partial tetrahedral or a partial octahedral orientation. The 5-fold coordination was reached by adding water molecules at the $Cu^{2+}$ ion (see Figure 3).

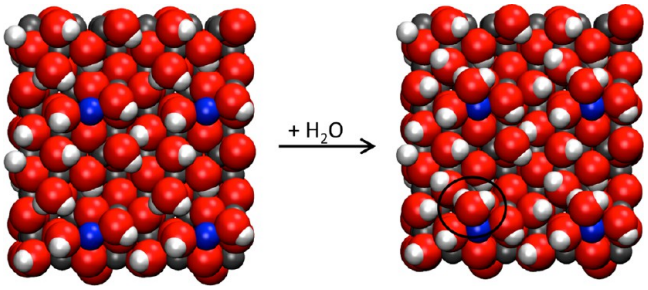


**Figure 3.** Modeling results showing that an additional water molecule is needed on top of the $Cu^{2+}$ to reach the experimental coordination. Shown are the best structures for the (110) surface at 7.1 $H_2O$/nm$^2$, without (left) and with (right) the additional water molecule on the copper. Note that, here and in consecutive figures, 2 × 2 unit cells are depicted.

Figure 4 shows that these additional water molecules indeed bind stronger than water molecules on the alumina surface itself. Thus, during drying it is the latter ones that are removed, not the ones on the copper. This is important, because it shows that these additional water molecules are present throughout the drying steps, until all hydration including the extra copper-coordinating water is lost at very high temperatures.

Figure 5 shows the adsorption energies of the $Cu^{2+}$ ions taking into account the additional water molecules. This is the ion exchange energy for the $Cu^{2+}$ ion plus the differential adsorption energy for the additional water molecules compared to adsorption on the empty surface. Note that these energies are relative to an arbitrary zero (gaseous $Cu(OH)_2$) and therefore have no absolute meaning. Comparing the adsorption energies for the different surfaces, we see that binding on the (111) surface is much weaker than binding on the (100) or (110) surface. Therefore, we conclude that $Cu^{2+}$ only binds on the (100) and the (110) surfaces. Looking at Figure 4, we notice that for these two surfaces the experimental coordination with five neighbors is reproduced nicely. When the surfaces are dried further, and the hydration comes below ca. 5 water molecules/nm$^2$, we find structures with only four oxygen neighbors at the $Cu^{2+}$.[59] Typical structures are shown in Figure 6.

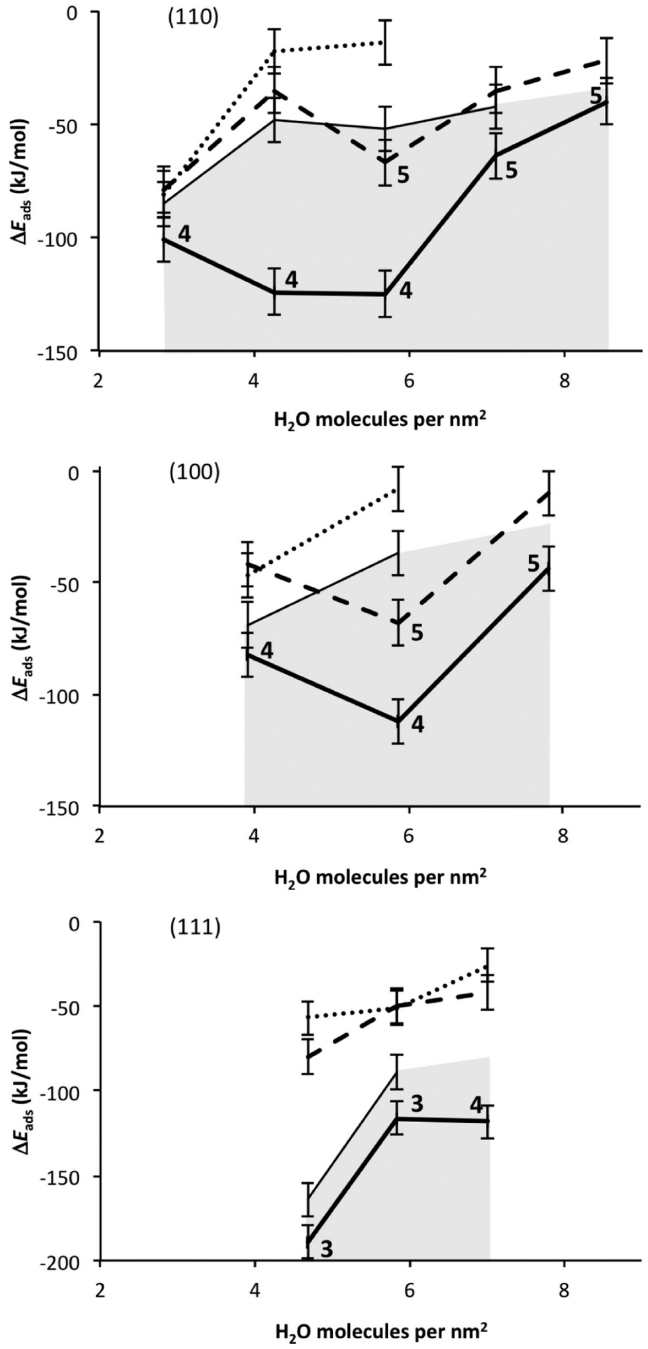


**Figure 4.** Adsorption energies of one, two, or three (respectively full, dashed, and dotted lines) additional water molecules on the adsorbed $Cu^{2+}$ species on several $\gamma$-alumina surfaces and at several levels of surface hydration. The thin lines denote the adsorption energy on the alumina surface itself (without the presence of $Cu^{2+}$). When the adsorption energies of the additional waters are in the gray area, the additional waters bind stronger to the copper than to the alumina surface itself, meaning that they are stable at the given level of hydration. The boldface numbers are the numbers of oxygen neighbors of the $Cu^{2+}$ ion. Note that the values on the abscissae are based on the hydration states before ion exchange (and before adding extra water molecules).

**Addition of $Cl^-$ Ions.** We calculated the exchange energy for the adsorption of $Cl^-$ to the (100), (110), and (111) surfaces without $Cu^{2+}$ at all hydration levels. The structures and energies are in good agreement with the results in ref 53. The


dx.doi.org/10.1021/cs400253w | ACS Catal. 2013, 3, 1545−1554

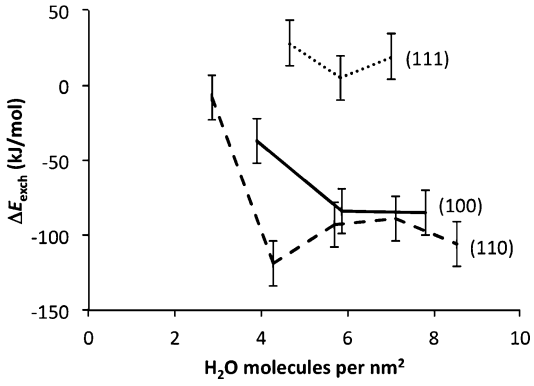


**Figure 5.** Exchange energies for the adsorption of $Cu^{2+}$ (plus additional water molecules) on various $\gamma$-alumina surfaces as a function of surface hydration. Energies are calculated according to eq 4 plus the differential adsorption energy of the additional water molecules compared to adsorption on the corresponding alumina surface.

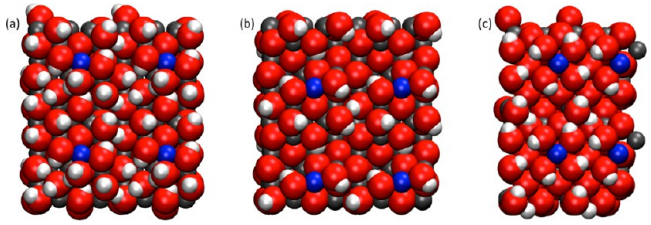


**Figure 6.** Typical structures of $Cu^{2+}$ ions on $\gamma$-alumina surfaces. Shown are the best structures for (a) the (110) surface at 8.5 $H_2O/nm^2$, (b) the (110) surface at 4.3 $H_2O/nm^2$, and (c) the (100) surface at 5.9 $H_2O/nm^2$. Note that in b the extra water is split into two OH groups.

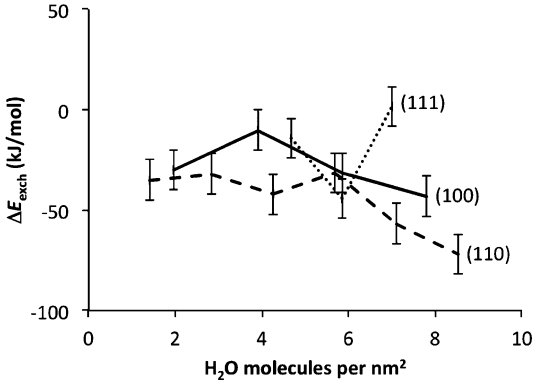


**Figure 7.** Exchange energies for the adsorption of $Cl^-$ on various $\gamma$-alumina surfaces as a function of the number of water molecules on the surface.

exchange energies (following eq 5) of the best structure on each surface at each hydration level are shown in Figure 7. Again, as for $Cu^{2+}$, there is a preference for the (110) surface, but for $Cl^-$ the (100) and (111) surfaces are within reach and are possibly also occupied. However, at full hydration the (111) surface is well-packed and the chloride ions hardly bind. Therefore, as the impregnation obviously takes place at (more than) full hydration, we suggest that after impregnation and drying, the (111) surface is chloride-free. This means that both the $Cu^{2+}$ and $Cl^-$ ions are present only on the (110) and (100) surfaces.

We also calculated the exchange energy for adsorption of chlorides on top of the adsorbed $Cu^{2+}$ ions. Figure 8 shows the

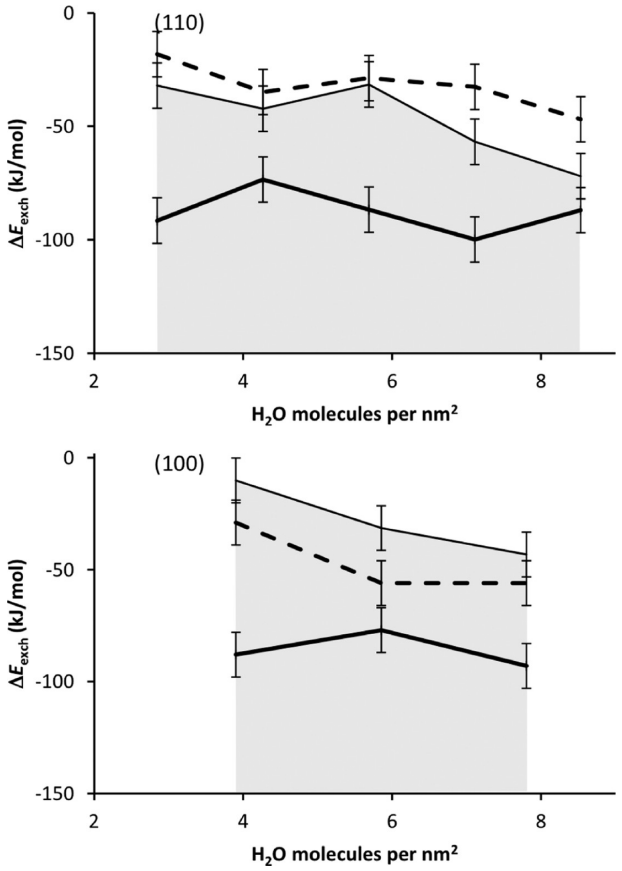


**Figure 8.** Exchange energies for the adsorption of one or two (respectively full and dashed lines) $Cl^-$ ions on top of $Cu^{2+}$ ions adsorbed on various $\gamma$-alumina surfaces as a function of surface hydration. The thin lines denote the adsorption on pristine alumina (no copper).

comparison with adsorption of chlorides on pristine alumina. We see clearly that the first $Cl^-$ actually prefers to bind on top of $Cu^{2+}$, rather than somewhere else on the alumina surface. For the second $Cl^-$ this depends on the surface: On the (110) surface, the second chloride prefers to bind on the alumina. Thus, thermodynamically, $CuCl^+$ will form and the other $Cl^-$ will adsorb separately, in practice reducing the number of binding sites for $Cu^{2+}$ by a factor of 2 (instead of 3). Conversely, on the (100) surface both chlorides prefer binding to the $Cu^{2+}$, forming isolated $CuCl_2$ species. Three typical structures are shown in Figure 9.

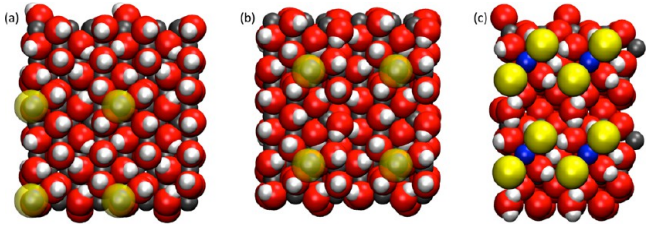


**Figure 9.** Typical structures for chloride bonded to adsorbed $Cu^{2+}$. Shown are the best structures for (a) the (110) surface at 8.5 $H_2O/nm^2$, (b) the (110) surface at 7.1 $H_2O/nm^2$, and (c) the (100) surface at 5.9 $H_2O/nm^2$. In a and b, the chlorines have been made semitransparent to show the copper below.


dx.doi.org/10.1021/cs400253w | ACS Catal. 2013, 3, 1545−1554

Note that these exchange energies are calculated in the presence of one or two additional water molecules at the $Cu^{2+}$. Note that when a chloride replaces one of the waters, the optimal number of additional waters may vary slightly: for the (100) surface it is the same; for the (110) surface, for all hydration levels except the fully hydrated one, now two additional waters bind to the $Cu^{2+}$ (of which one is replaced by $Cl^-$).

Similarly as above, we can estimate at what temperatures HCl would desorb under heating. For gaseous HCl, the standard entropy is 186.8 J/mol K[60] with a temperature dependence of $S = a + 3.5R \ln T$. For the adsorbed state, we used—rather arbitrarily—the same value as for water. For the dehydrated (100) surface, the HCl desorption energy is 142 kJ/mol, thus predicting desorption at 800 K. For the dehydrated (110) surface, it is 224 kJ/mol and 1190 K, respectively. For HCl desorption from $CuCl^+(OH^-)$ on the dehydrated (110) surface, we found 284 kJ/mol and 1460 K.

**Analysis of the Best Structures.** Analyzing the best structures at different hydration levels with and without chlorides, we see that the positions of the copper ions vary (here we will discuss only the structures with the correct number of additional water molecules as described above, but even then the best positions are scattered all over the unit cells). Moreover, the energy differences between the best and second best copper positions can differ for different hydration levels by up to 0.8 eV, and in many cases there are alternative structures within 0.1 eV. This means there is no single preferred binding site for $Cu^{2+}$ on the $\gamma$-alumina, agreeing with the experimental observation that there must be "at least two slightly different structures."[13]

This is especially true for the (100) surface, where the copper positions are scattered. The (110) surface is slightly more orderly: only two positions alternate having the best energy when no $Cl^-$ is present. But still other alternatives are close in energy as well (within 0.2 eV).

The same holds for the chloride positions on alumina (without copper): There is no single preferred position for all hydration levels, and alternatives differ little in energy (Figure 10). For roughly half of the (110) surfaces, the best positions for $Cu^{2+}$ and for $Cl^-$ overlap, but in the other cases they do not. This means that the theory that the copper and chloride ions exclude each other because they prefer binding at or close to the same sites[13] cannot be confirmed from our calculations. It may be, however, that in solution the preferred sites are more well-defined and do overlap.

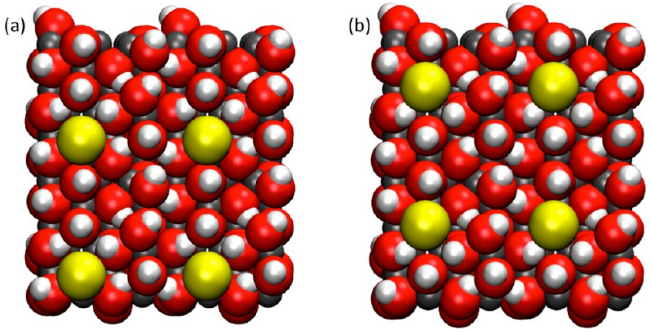


**Figure 10.** The best and the second best positions for chlorides on the (110) surface of $\gamma$-alumina at 8.5 $H_2O/nm^2$. The energy difference between these two structures is only 0.06 eV (6 kJ/mol).

Examining the local structures further, we see that all best structures without chlorides do have a comparable copper coordination: an octahedral symmetry with five oxygen neighbors and one vacancy. All these structures also show a clear Jahn–Teller effect, with distances in the following ranges: the axial oxygen is at 2.17–2.65 Å, short equatorial distances usually are 1.95–2.02 Å, and long equatorial distances usually are 2.02–2.27 Å.

On the (100) surface the copper is always bonded to one alumina oxygen (with three aluminum neighbors), three surface OH groups, and one additional water molecule. Most aluminum neighbors have six neighbors themselves. On the (110) surface, the copper typically sits slightly deeper, binding to two alumina oxygens, two surface OH groups, and one additional water. Here the alumina oxygens involved usually have only two aluminum neighbors ($\mu_2$), and these aluminum ions often have less than six neighbors.

For the structures with one chloride ((110) surface) or two chlorides ((100) surface) on the copper, we see that often different positions are preferred, and that the copper is pulled somewhat out of the surface. On the (110) surface, the copper now has only one alumina oxygen neighbor, plus three surface OH neighbors and one $Cl^-$ neighbor, not necessarily in octahedral symmetry anymore. Here the chloride is perpendicular to the surface. Conversely, on the (100) surface the copper-bound chloride ions more readily accept hydrogen bonds from the surface OH groups. This may explain why for this surface both chloride ions prefer binding to the copper. In such structures, the copper even sticks out, and its bond toward the one alumina oxygen elongates to ≥2.6 Å.

**Comparison with Literature Results.** Comparing our results with those of Leofanti et al.,[13,32] we note several differences: The experiments give one distance (1.94 ± 0.01 Å) for all five Cu–O interactions, and a symmetric coordination is claimed based on EPR measurements. We find clearly asymmetric coordinations with somewhat longer distances. Our average equatorial Cu–O distance is 2.03 Å, about 5% longer than the distance reported by Leofanti et al. This suggests that the rPBE-optimized distances are somewhat too long. For applications for which the average absolute Cu–O distance is important, the experimental value is probably the most accurate one. However, for future calculations on the fate of the adsorbed ions, one should use the computationally optimized structures, so that the calculations are self-consistent.

The claim of symmetry we do not understand. From inorganic chemistry it is known that $Cu^{2+}$ prefers an asymmetric coordination, so, especially on the strongly disordered $\gamma$-alumina surfaces, it is unlikely that it would have symmetric surroundings. Probably the experimental measurements are averaged over many slightly different binding sites.

More importantly, EXAFS measurements show no Cu–Cl interactions, but we find that half of the chlorides should be on the alumina and half should be coordinated at the copper. Our interpretation of this difference is that in solution the $Cu^{2+}$ and $Cl^-$ ions probably do prefer binding to the surface as separate ions (supported by the fact that $CuCl_2$ dissociates when dissolved in water), and on the dried (but still hydrated) surfaces the thermodynamic optimum is formation of $CuCl^+$ species (and $CuCl_2$ in case of the (100) surface). Probably the formation of $CuCl^+$ species during the drying process is kinetically hindered, and thus the thermodynamic optimum of our calculations is not reached in practice. Hence, we predict that the structure with dissociated copper and chloride ions, as


dx.doi.org/10.1021/cs400253w | ACS Catal. 2013, 3, 1545–1554

found after drying, is metastable. Heating it will make the chloride ions diffuse and bind to the copper ions. The experimental structure after only drying is described well by our structures before adding chlorides. Incidentally, concerning the copper positions and coordination, this is also a proper model for the structure formed when impregnating with copper nitrate; the only difference is that with copper chloride 2/3 of the binding sites are taken by chlorides.

**Experimental Confirmation.** We designed experiments to test the conclusions of our calculations, namely that $CuCl^+$ species (on the (110) surface) and $CuCl_2$ species (on the (100) surface) will form when the ions are given the chance to diffuse by applying heat. We prepared samples and compared temperature programmed desorption (TPD) and reduction (TPR) patterns before and after heating them. The results are remarkable: When the samples are heated to high temperatures using a fast heating rate (10 K/min), the ions do not get the chance to diffuse over the surface, and the chloride is lost to the gas phase as HCl. But when the samples are kept at an intermediate temperature long enough, the chloride ions move to the copper ions. As they bind much stronger to the copper ions than to the alumina surface, these chloride ions are not lost anymore to the gas phase upon further heating.

Figures 11 and 12a show the TPD and TPR patterns of the original only dried samples. The TPD pattern consists of two

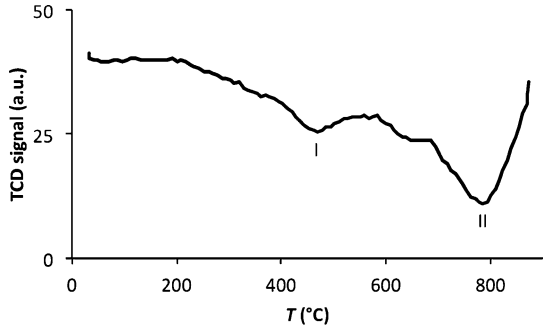


**Figure 11.** Temperature programmed desorption (TPD) plot for $CuCl_2$ on $\gamma$-alumina (1.5 wt % Cu). Desorbing HCl is plotted as a negative signal.

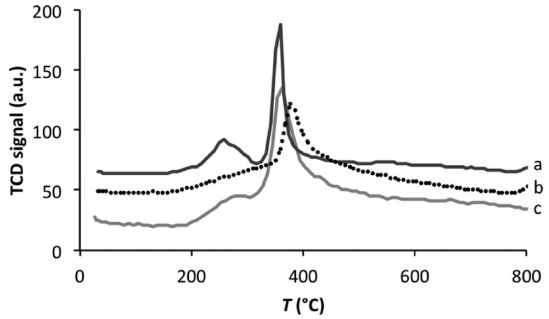


**Figure 12.** Temperature programmed reduction (TPR) plots for (a) the original only dried sample, (b) after pretreating the sample at 400 °C, and (c) after measuring the TPD pattern (i.e., after fast heating to 900 °C), scaled to sample mass. $H_2$ consumption is plotted as positive signal.

main peaks of desorbing HCl, the temperatures of which fit nicely with the binding energies of $Cl^-$ on the (100) and (110) surfaces (peaks I and II, respectively). The TPR pattern also consists of two peaks (of opposite direction), showing $H_2$ consumption and therefore indicating copper reduction. According to Rouco,[30] the first peak denotes reduction of $Cu^{II}$ to $Cu^{I}$, and the second one denotes reduction of $Cu^{I}$ to $Cu^0$.

When the sample is heated to 400 °C for one hour, the chloride ions diffuse to the copper ions, changing the copper coordination and its reducibility. This is recognized in the clear change of the TPR pattern (Figure 12b). For comparison, we also performed TPR on a sample that was recovered after TPD and thus had already been heated to 900 °C (Figure 12c). The latter TPR pattern resembles that of the original only dried sample. This proves that the change after heating to 400 °C is not caused only by improved bonding of the copper ions with the alumina surface because of heating but that the copper coordination must have changed. In other words, the chloride ions moved to the copper ions.

Finally, Figure 13 shows the TPD pattern after treatment at 400 °C. If the chloride ions have moved to the copper ions,

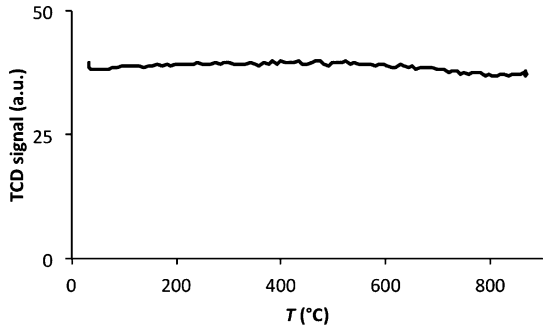


**Figure 13.** Temperature programmed desorption (TPD) plot for the sample after pretreatment at 400 °C. This sample does not show any HCl desorption.

they are now bonded much stronger than at the alumina surface. As a result, their desorption temperatures should increase. Indeed, Figure 13 shows no desorption of HCl up to 900 °C, confirming once again that the chloride ions have moved to the copper ions.

Note that apparently all chlorides have moved to the copper ions, suggesting that also on the (110) surface $CuCl_2$ species have formed and not merely $CuCl^+$ species. To understand this, we should realize that at 400 °C the (110) surface is partly dehydrated and contains at most four $H_2O$ molecules per $nm^2$ (see Figure 2 and the discussion above). In this hydration state, the preference for $CuCl^+$ over $CuCl_2$ is not significant, and apparently at this temperature $CuCl_2$ species are preferred after all.

**Discussion.** The surface hydration is important for the binding mode of adsorbing ions. Importantly, we found that additional water molecules stay coordinated to the copper ion at both high and low levels of hydration. This means that finding the correct structures is impossible without explicitly adding these water molecules. These additional water molecules will also affect the calcination processes: Molecules on top of a metal ion will influence the diffusion of the ion, changing the size of particles formed during calcination. It is very likely that this pertains to other metal ions as well, so in this type of modeling it should always be tested whether additional water molecules may be present and should be added.

In this work, we bypassed the impregnation process to prevent modeling of complicated systems with explicit liquid


dx.doi.org/10.1021/cs400253w | ACS Catal. 2013, 3, 1545−1554

water and ionic strength effects. These would need very long MD simulations. Therefore, we assumed that the system will find its thermodynamic optimum and the correct structure after drying can be found by searching the most stable structure of the ions on a dry/hydrated surface. Essentially, we assumed that (i) in solution the thermodynamically best binding sites are found by the ions and (ii) that during drying either the best binding sites stay the same or moving to the best dry binding sites is not kinetically hindered.

Considering our findings, the presence of the additional water molecule on top of the copper ion can hardly be kinetically limited as before drying there are water molecules everywhere. On the other hand, the formation of $CuCl^+$ and $CuCl_2$ species on the surface during drying probably has kinetic barriers. Since both copper and chloride ions bind strongly to the $\gamma$-alumina surface, the diffusion of either should incur relatively high barriers. Moreover, probably the formation of $CuCl^+$ and $CuCl_2$ is only favored when almost all the liquid water has been removed. At this stage, diffusion of ions to form $CuCl^+$ species is a comparable process to the diffusion of ions to form metal oxide nanoparticles. This process does not happen during drying but during calcination at higher temperatures. Our experiments show that, indeed, upon heating the chloride ions move to the copper ions. Notably, this only happens at moderate heating: when the samples are heated to a high temperature at a high heating rate, the chlorides are lost to the gas phase as HCl. Thus, both our calculations and our experiments show that during calcination, copper and chloride ions will recombine and may diffuse not only separately but also as $CuCl^+$ and $CuCl_2$. The specific balance between these processes depends on the heating rate.

Finally, we mention that the true binding structures of ions on an alumina surface should not be considered as one best local structure that will be formed all over the surface. Even when ignoring the amorphic nature of $\gamma$-alumina, a range of best structures will be visited depending on the temperature, according to a Boltzmann distribution.

Our method of searching for best structures gives a range of best structures as well. However, some good structures are missed. During the geometry optimizations, the hydrogen bond network does not easily adapt to the presence of the ions, while it is known (and also visible in our calculations) that the optimal hydrogen bond network can vary.[54] To be sure that all possible best structures are found, it is necessary to use many variations of the hydration structure as starting points for the ion exchange and optimizations. Moreover, the thresholds of 1.0, 0.7, and 0.5 eV that we used for selecting structures may be too strict and can cause good structures to be missed. However, in order to keep the number of calculations feasible (ca. 10000 in the current project), we must accept the possibility of missing structures.

An alternative method that may be more efficient is explorative MD.[39,40] This method does not explore combinations of possibilities like we did, but explores the space of possibilities by very rough molecular dynamics, restricting unwanted degrees of freedom. An added advantage, apart from efficiency, is that the exploration is not limited by the creativity of the person constructing the possibilities, such as the addition of extra water molecules in our case. However, in our case, the hydration layer would evaporate under such high temperature MD. As this is the layer we want to sample, its evaporation cannot be prevented by fixating these atoms, and additional tricks would need to be invented. Therefore, in its current form, explorative MD is not the optimal tool for us.

## CONCLUSION

Our calculations suggest that both $Cu^{2+}$ and $Cl^-$ adsorb exclusively on the (110) and (100) surfaces of $\gamma$-alumina, and not on the (111) surface. Moreover, there are additional water molecules on the copper ions. As these water molecules are very likely to affect the calcination process, investigating the presence of such additional water molecules is crucial for correct modeling of metal ions adsorbing on a support.

Furthermore, we find that chloride ions prefer to adsorb on the copper ion rather than elsewhere on the surface. On the (100) surface, both chloride ions bind to the copper. On the (110) surface, only one chloride binds to the copper, and the other does bind to the alumina surface. In experimental work in the literature on only dried samples, the chlorides are not found on the copper ions, so we conclude that the formation of the thermodynamic optimum as found with our models is kinetically hindered, and during drying the ions stay in the dissociated state that was optimal during impregnation. When the ions get the chance to diffuse during calcination, the predicted $CuCl^+$ and $CuCl_2$ species will form, before they diffuse further to form $CuCl_2$ nanoparticles. Importantly, we confirmed this theoretical prediction in the laboratory.

## AUTHOR INFORMATION

### Corresponding Author

*E-mail: m.j.louwerse@uva.nl.

### Notes

The authors declare no competing financial interest.

## ACKNOWLEDGMENTS

We thank the Dutch National Research School Combination Catalysis (NRSC-C) for funding.

## REFERENCES

(1) Schwarz, J. A.; Contescu, C.; Contescu, A. *Chem. Rev.* **1995**, *95*, 477.
(2) Perego, C.; Villa, P. *Catal. Today* **1997**, *34*, 281.
(3) Pinna, F. *Catal. Today* **1998**, *41*, 129.
(4) Toebes, M. L.; van Dillen, J. A.; de Jong, K. P. *J. Mol. Catal. A: Chem.* **2001**, *173*, 75.
(5) Marceau, E.; Carrier, X.; Che, M. In *Synthesis of Solid Catalysts*; de Jong, K. P., Ed.; Wiley-VCH: Weinheim, Germany, 2009.
(6) Batyrev, E. D.; Shiju, N. R.; Rothenberg, G. *J. Phys. Chem. C* **2012**, *116*, 19335.
(7) Caro, C.; Thirunavukkarasu, K.; Anilkumar, M.; Shiju, N. R.; Rothenberg, G. *Adv. Synth. Catal.* **2012**, *354*, 1327.
(8) Lobo-Lapidus, R. J.; Gates, B. C. *J. Catal.* **2009**, *268*, 89.
(9) Green, I. X.; Tang, W.; Neurock, M.; Yates, J. T., Jr. *Science* **2011**, *333*, 736.
(10) Bourikas, K.; Kordulis, C.; Lycourghiotis, A. *Catal. Rev.* **2006**, *48*, 363.
(11) Panagiotou, G. D.; Petsi, T.; Bourikas, K.; Garoufalis, C. S.; Tsevis, A.; Spanos, N.; Kordulis, C.; Lycourghiotis, A. *Adv. Colloid Interface Sci.* **2008**, *142*, 20.
(12) Rachel, A.; Kumari, V. D.; Subramanian, R.; Chary, K. V. R.; Rao, P. K. *Indian J. Chem. A* **2004**, *43*, 1172.
(13) Leofanti, G.; Padovan, M.; Garilli, M.; Carmello, D.; Zecchina, A.; Spoto, G.; Bordiga, S.; Turnes Palomino, G.; Lamberti, C. *J. Catal.* **2000**, *189*, 91.
(14) Argyle, M. D.; Chen, K.; Bell, A. T.; Iglesia, E. *J. Catal.* **2002**, *208*, 139.

(15) Shiju, N. R.; Anilkumar, M.; Mirajkar, S. P.; Gopinath, C. S.; Rao, B. S.; Satyanarayana, C. V. *J. Catal.* **2005**, *230*, 484.
(16) Feng, H.; Elam, J. W.; Libera, J. A.; Pellin, M. J.; Stair, P. C. *J. Catal.* **2010**, *269*, 421.
(17) Hu, H.; Wachs, I. E.; Bare, S. R. *J. Phys. Chem.* **1995**, *99*, 10897.
(18) Kijlstra, W. S.; Poels, E. K.; Bliek, A.; Weckhuysen, B. M.; Schoonheydt, R. A. *J. Phys. Chem. B* **1997**, *101*, 309.
(19) Ataloglou, T.; Vakros, J.; Bourikas, K.; Fountzoula, C.; Kordulis, C.; Lycourghiotis, A. *Appl. Catal. B: Environ.* **2005**, *57*, 299.
(20) Kumar, M. S.; Hammer, N.; Rønning, M.; Holmen, A.; Chen, D.; Walmsley, J. C.; Øye, G. *J. Catal.* **2009**, *261*, 116.
(21) Gervasini, A.; Manzoli, M.; Martra, G.; Ponti, A.; Ravasio, N.; Sordelli, L.; Zaccheria, F. *J. Phys. Chem. B* **2006**, *110*, 7851.
(22) Villadsen, J.; Livbjerg, H. *Catal. Rev.: Sci. Eng.* **1978**, *17*, 203.
(23) Muddada, N. B.; Olsbye, U.; Caccialupi, L.; Cavani, F.; Leofanti, G.; Gianolio, D.; Bordiga, S.; Lamberti, C. *Phys. Chem. Chem. Phys.* **2010**, *12*, 5605.
(24) Garcia, C. L.; Resasco, D. E. *J. Catal.* **1990**, *122*, 151.
(25) Liu, J.; Lu, X.; Zhou, G.; Zhen, K.; Zhang, W.; Cheng, T. *React. Kinet. Catal. Lett.* **2006**, *88*, 315.
(26) Baiker, A.; Monti, D.; Wokaun, A. *Appl. Catal.* **1986**, *23*, 425.
(27) Sermon, P. A.; Rollins, K.; Reyes, P. N.; Lawrence, S. A.; Martin Luengo, M. A.; Davies, M. J. *J. Chem. Soc., Faraday Trans. 1* **1987**, *83*, 1347.
(28) Garcia, C. L.; Resasco, D. E. *Appl. Catal.* **1989**, *46*, 251.
(29) Bond, G. C.; Namijo, S. N.; Wakeman, J. S. *J. Mol. Catal.* **1991**, *64*, 305.
(30) Rouco, A. J. *Appl. Catal. A: Gen.* **1994**, *117*, 139.
(31) Leofanti, G.; Padovan, M.; Garilli, M.; Carmello, D.; Marra, G. L.; Zecchina, A.; Spoto, G.; Bordiga, S.; Lamberti, C. *J. Catal.* **2000**, *189*, 105.
(32) Prestipino, C.; Bordiga, S.; Lamberti, C.; Vidotto, S.; Garilli, M.; Cremaschi, B.; Marsella, A.; Leofanti, G.; Fisicaro, P.; Spoto, G.; Zecchina, A. *J. Phys. Chem. B* **2003**, *107*, 5022.
(33) Krokidis, X.; Raybaud, P.; Gobichon, A.-E.; Rebours, B.; Euzen, P.; Toulhoat, H. *J. Phys. Chem. B* **2001**, *105*, 5121.
(34) Paglia, G.; Rohl, A. L.; Buckley, C. E.; Gale, J. D. *Phys. Rev. B* **2005**, *71*, 224115.
(35) Digne, M.; Sautet, P.; Raybaud, P.; Euzen, P.; Toulhoat, H. *J. Catal.* **2002**, *211*, 1.
(36) Digne, M.; Sautet, P.; Raybaud, P.; Euzen, P.; Toulhoat, H. *J. Catal.* **2004**, *226*, 54.
(37) Briquet, L. G. V.; Catlow, C. R. A.; French, S. A. *J. Phys. Chem. C* **2009**, *113*, 16747.
(38) Shi, X. R.; Sholl, D. S. *J. Phys. Chem. C* **2012**, *116*, 10623.
(39) Mager-Maury, C.; Bonnard, G.; Chizallet, C.; Sautet, P.; Raybaud, P. *ChemCatChem* **2011**, *3*, 200.
(40) Mager-Maury, C.; Chizallet, C.; Sautet, P.; Raybaud, P. *ACS Catal.* **2012**, *2*, 1346.
(41) Ordejon, P.; Artacho, E.; Soler, J. M. *Phys. Rev. B* **1996**, *53*, R10441.
(42) Soler, J. M.; Artacho, E.; Gale, J. D.; Garcia, A.; Junquera, J.; Ordejon, P.; Sanchez-Portal, D. *J. Phys.: Condens. Matter* **2002**, *14*, 2745.
(43) Hohenberg, P.; Kohn, W. *Phys. Rev.* **1964**, *136*, B864.
(44) Kohn, W.; Sham, L. J. *Phys. Rev.* **1965**, *140*, A1133.
(45) Hammer, B.; Hansen, L. B.; Norskov, J. K. *Phys. Rev. B* **1999**, *59*, 7413.
(46) Troullier, N.; Martins, J. L. *Phys. Rev. B* **1991**, *43*, 1993.
(47) Octopus pseudopotential generator: http://www.tddft.org/programs/octopus/pseudo.php.
(48) Louwerse, M. J.; Rothenberg, G. *Phys. Rev. B* **2012**, *85*, 035108.
(49) Sankey, O. F.; Niklewski, D. J. *Phys. Rev. B* **1989**, *40*, 3979.
(50) Wischert, R.; Copéret, C.; Delbecq, F.; Sautet, P. *Angew. Chem., Int. Ed.* **2011**, *50*, 3202.
(51) Wischert, R.; Laurent, P.; Copéret, C.; Delbecq, F.; Sautet, P. *J. Am. Chem. Soc.* **2012**, *134*, 14430.
(52) Digne, M.; Raybaud, P.; Sautet, P.; Guillaume, D.; Toulhoat, H. *Phys. Chem. Chem. Phys.* **2007**, *9*, 2577.
(53) Digne, M.; Raybaud, P.; Sautet, P.; Guillaume, D.; Toulhoat, H. *J. Am. Chem. Soc.* **2008**, *130*, 11030.
(54) Mason, S. E.; Iceman, C. R.; Tanwar, K. S.; Trainor, T. P.; Chaka, A. M. *J. Phys. Chem. C* **2009**, *113*, 2159.
(55) Eisenberg, D.; Kauzmann, W. *The Structure and Properties of Water*; Oxford University Press: Oxford, U. K., 1969.
(56) Campbell, C. T.; Sellers, R. V. *J. Am. Chem. Soc.* **2012**, *134*, 18109.
(57) Carrier, X.; Marceau, E.; Lambert, J.-F.; Che, M. *J. Colloid Interface Sci.* **2007**, *308*, 429.
(58) Ravenelle, R. M.; Copeland, J. R.; Kim, W.-G.; Crittenden, J. C.; Sievers, C. *ACS Catal.* **2011**, *1*, 552.
(59) This switching value is slightly higher than the hydration state we predicted in the previous subsection, suggesting that because of the $Cu^{2+}$, the hydration layer's interaction with the alumina became slightly stronger. However, we expect this effect to be too small to affect the analysis presented in Figure 4.
(60) *CRC Handbook of Chemistry and Physics*, 66th ed.; CRC Press: Boca Raton, FL, 1986.